HHS Public Access

Author manuscript

J Biomech. Author manuscript; available in PMC 2021 November 09.

Published in final edited form as:

J Biomech. 2020 November 09; 112: 110044. doi:10.1016/j.jbiomech.2020.110044.

Between-session Reliability of Subject-Specific Musculoskeletal Models of the Spine Derived from Optoelectronic Motion Capture Data

Katelyn Burkhart[1,2,3], **Daniel Grindle**[2,4], **Mary L. Bouxsein**[1,2,3], **Dennis E. Anderson**[2,3]

[1]Harvard-MIT Health Sciences and Technology Program, Massachusetts Institute of Technology, Cambridge 02139, Massachusetts

[2]Center for Advanced Orthopaedic Studies, Beth Israel Deaconess Medical Center, 330 Brookline Ave., Boston 02215, Massachusetts

[3]Department of Orthopaedic Surgery, Harvard Medical School, Boston 02115, Massachusetts

[4]Division of Engineering Mechanics, Department of Biomedical Engineering and Mechanics, Virginia Polytechnic Institute and State University, Blacksburg, VA, United States

Abstract

This study evaluated the between-session reliability of creating subject-specific musculoskeletal models with optoelectronic motion capture data, and using them to estimate spine loading. Nineteen healthy participants aged 24–74 years underwent the same set of measurements on two separate occasions. Retroreflective markers were placed on anatomical regions, including C7, T1, T4, T5, T8, T9, T12 and L1 spinous processes, pelvis, upper and lower limbs, and head. We created full-body musculoskeletal models with detailed thoracolumbar spines, and scaled these to create subject-specific models for each individual and each session. Models were scaled from distances between markers, and spine curvature was adjusted according to marker-estimated measurements. Using these models, we estimated vertebral compressive loading for five different standardized postures: neutral standing, 45° trunk flexion, 15° trunk extension, 20° lateral bend to the right, and 45° axial rotation to the right. Intraclass correlation coefficients (ICCs) and standard error of measurement were calculated as measures of between-session reliability and measurement error, respectively. Spine curvature measures showed excellent reliability (ICC= 0.79–0.91) and body scaling segments showed fair to excellent reliability (ICC = 0.46–0.95). We found that musculoskeletal models showed mostly excellent between-session reliability to estimate spine loading, with 91% of ICC values > 0.75 for all activities. This information is a necessary precursor for using motion capture data to estimate spine loading from subject-specific musculoskeletal models, and suggests that marker data will deliver reproducible subject-specific models and estimates of spine loading.

Conflict of Interest

There are no conflicts of interest.

Keywords

Spine loading; Motion analysis; Repeatability; Musculoskeletal model; Model scaling

Introduction

Musculoskeletal models simulating complex spinal anatomy have been developed to better understand internal spinal loading conditions during daily living activities.(Beaucage-Gauvreau et al., 2019; Bruno et al., 2017a; Ignasiak et al., 2018) Optoelectronic motion capture systems are commonly used to provide data input for scaling of musculoskeletal models to an individual's specific anthropometry. However, there is a known error in optoelectronic motion capture due to inherent system performance(Richards, 1999) and more notably due to variation in marker placement on anatomical landmarks (Della Croce et al., 1999; Krumm et al., 2016; Rast et al., 2016). While these concerns have been well studied in gait models, there has been limited prior investigation into how this variation might affect marker-estimated spine models and spinal loading predictions.

While several detailed full-body lumbar spine models exist in the OpenSim community(Actis et al., 2018; Beaucage-Gauvreau et al., 2019; Raabe and Chaudhari, 2016), the only detailed thoracolumbar spine model(Bruno et al., 2015) does not incorporate lower extremities. A full-body model is necessary for use in typical motion analysis applications so that ground reaction forces can be applied to the model and whole-body motion can be analyzed. A detailed full-body musculoskeletal model would allow for prediction of thoracolumbar spine loading and trunk muscular activations during different activities, and could help inform future studies investigating biomechanical mechanisms behind multiple diseases and conditions including vertebral fracture, scoliosis, back pain, and hyperkyphosis. Therefore, the aim of this study was to investigate how variation in the placement of anatomical markers affects the reliability of body segment scaling, estimated spine curvature, and resulting compressive spine loading outcomes when creating subject-specific musculoskeletal models.

Methods

Creation of Full-Body Musculoskeletal Model

We created a full-body model of the thoracolumbar spine by combining our previously validated male and female thoracolumbar spine models (Bruno et al., 2017a, 2015) with a published gait model (Gait2354)(Anderson and Pandy, 2001, 1999; Carhart, 2000; Delp et al., 1990; Yamaguchi and Zajac, 1989). These models were developed using the OpenSim musculoskeletal modeling software (Delp et al., 2007) and include 552 and 54 individual muscle fascicles, respectively. During model combination, the pelvis and sacrum bodies were kept from the spine models, while lower extremity segments (femur, tibia/fibula, talus, calcaneus and toes) were introduced from the gait model. Pelvis and sacrum center of mass (CoM) locations were used from the Gait2354 model, as these parameters were based on more comprehensive anatomical sources. The hip joint, formerly connected to ground, was modified to connect the pelvis body to the femur (on the right and left) with

three degrees-of-freedom. The pelvis-ground joint was changed to a kinematic joint that positions the model in space relative to the ground and allows for 6 degrees of freedom (3 rotational and 3 translational). The ankle joint was modified to be a pin joint (with one degree-of-freedom), allowing only dorsiflexion and plantar flexion, and the toe joint was modified to be a weld joint, allowing no movement at the midfoot. Markers were attached to the model bodies corresponding to the experimental marker set used in data collections.

To match the anthropometry of the male and female thoracolumbar models, we scaled the mass and length properties of the legs to that of a 78kg, 1.75m male and 61kg, 1.63m female, respectively(De Leva, 1996; Liu et al., 1971; Pearsall et al., 1996). Inertial properties of the lower extremity bodies, as incorporated from the gait model, were scaled according to each body's corresponding mass and length changes. Inertial properties for the arms, and thoracic and lumbar segments (represented as a slice through the trunk at a spinal level) were added from literature, after scaling for height and weight of our male and female models (De Leva, 1996; Pearsall et al., 1996). The psoas muscle spans from the thoracolumbar spine to the femur. As such, the psoas fascicles were modified from the thoracolumbar models to have their distal fixed attachments occur on the lesser trochanter of the femur and a conditional via point on the pelvis, as adapted from the Gait2354 model. Other lower limb musculature was incorporated directly from the gait model, while any fascicles that connected the pelvis to the torso were excluded as these muscles already exist in the thoracolumbar models. The resulting full-body models include 598 Hill-type muscle fascicles and 108 degrees-of-freedom (Figure 1).

Participants

Nineteen healthy adult volunteers (11 male, 8 female) were recruited for this study. The mean ± SD (range) age, height, weight and BMI of the participants were: 47 ± 17 (24–74) years, 172 ± 7 (162–184) cm, 71 ± 14 (45–98) kg, and 24.0 ± 3.3 (16.8–30.9) kg/m^2 respectively. Individuals were excluded if they experienced recent back pain, or had a history of spinal surgery or traumatic fracture, thoracic deformity, or conditions that affect balance and movement. This study was approved by the Institutional Review Board of Beth Israel Deaconess Medical Center. All participants provided written informed consent before their study session.

Procedure

Subjects participated in the same set of measurements on two separate occasions, an average of 8 days apart (range: 2–17 days). The data collection procedure was previously published(Mousavi et al., 2018). At the start of each session, height and weight were documented. Anatomical landmarks were palpated and retroreflective markers were attached to the skin using double-adhesive tape. Rigid clusters with four markers each were attached over the palpated T1, T4, T5, T8, T9, T12 and L1 spinous processes. Markers were placed over anatomic landmarks on the pelvis, including the posterior (PSIS) and anterior (ASIS) superior iliac spines and iliac crests. Additional markers were placed on C7 and bilaterally on the acromion (shoulder), lateral epicondyle of the humerus (elbow), radial styloid process (wrist), greater trochanter of the femur, lateral and medial aspects of the knee joint, lateral and medial aspects of the ankle joint, posterior heel and first metatarsophalangeal (MTP)

joint (big toe). A headband with four markers attached was used to track head motion, and 41 other markers were placed on the sternum, clavicles and extremities. A 10-camera motion analysis system (Vicon Motion Systems, Oxford, UK) was used to collect marker data in a neutral upright standing position. Subjects were instructed to stand upright with one foot on each force plate and keep their arms at their sides.

Data Processing

Marker positions were averaged over each neutral standing trial to obtain static marker positions. Additional estimated virtual markers and joint centers were calculated from existing measured marker data. Hip joint centers, and intervertebral joints from C7/T1 to L5/S1 were estimated from marker data using published methods(Nerot et al., 2018; Peng et al., 2015). The knee and ankle joint centers were calculated as the midpoint between the medial and lateral joint landmarks. A centralized ‘head’ marker was estimated as the centroid of the 4 external headband markers. Lastly, mid-PSIS and mid-hip joint center markers were created as the midpoint between these existing markers.

Subject-Specific Model Creation

The male or female full-body thoracolumbar spine model, as appropriate, was scaled to the anthropometry of each participant, using height, weight, and distance between anatomical landmarks or marker-derived joint centers measured during the static neutral standing trial of each session. Intervertebral joint centers, as derived from marker data, were used to set spine curvature for each participant during each session. Height and weight were scaled using previously described methods (Bruno et al., 2017b). Overall thoracic kyphosis was calculated from the model as the angle between T4 and T12 vertebral bodies, similar to the classic Cobb angle approach. Overall lumbar lordosis was calculated from the model as the angle between L1 and L5 vertebral bodies. Body segment scaling factors were applied as described in Table 1. A height scale factor was used if a body segment was not scaled from marker-measured distances. Absolute body segment measurements were calculated by multiplying the body scale factor with the original body segment length in the musculoskeletal model.

Spine Loading Simulations

We used the same prescribed motions for all subjects to investigate the reliability of spine loading between sessions evaluated by subject-specific thoracolumbar spine models created with marker-based motion capture data. For each subject-specific model, we estimated vertebral compressive loading for five standardized postures: neutral standing, 45° trunk flexion, 15° trunk extension, 20° lateral bend to the right, and 45° axial rotation to the right. Trunk motions were distributed through the intervertebral joints and pelvis from reported literature ratios for flexion/extension, lateral bending and axial rotation, as previously described (Bruno et al., 2015), and identical kinematics were applied to all subjects.

Static optimization and joint reaction analyses were performed with OpenSim (version 3.3) via custom Matlab scripts to estimate muscle and joint reaction forces and simulated ground reaction forces. Force and torque residual actuators were applied between the ground and left/right calcanei to simulate ground reaction forces between the feet and floor. Our

optimization routine minimized the sum of cubed muscle activations, and joint reaction calculations were used to estimate the compressive force applied to each vertebral body during activities(Bruno et al., 2015).

Statistical Analyses

Primary outcomes were magnitude and reliability of segment scaling factors, marker-estimated thoracic and lumbar spine curvatures, and spine loading. Reliability of each outcome was examined using intraclass correlation coefficients (ICC) and classified as excellent (ICC>0.75), fair (0.4<ICC<0.75) or poor (ICC<0.4)(Shrout and Fleiss, 1979). Standard error of measurement (SEM) as a parameter of absolute reliability indicates magnitude of error and within-subject variability across repeated trials, and was calculated as:

$$SEM = SD\sqrt{1 - ICC}$$

where SD is standard deviation of the measurement. Analyses were performed with MATLAB (The Mathworks Inc., Natick, MA) and Prism (GraphPad Software Inc., CA, USA).

Results

Of the nineteen healthy subjects, two subjects were excluded from analysis due to missing or hidden retroreflective markers on the ASIS of the pelvis or on the L1 vertebral body. For body segment scaling, mean differences between sessions were not different than zero ($p>0.05$) (Figure 2 and 3). The measurements with excellent reliability (ICC > 0.75) were the head and neck length and width, humeri and radii, spine and foot length and width (Table 2). All other scaling measurements had fair reliability with ICCs ranging from 0.46 – 0.75. For the full 95% confidence interval range of the ICC, all scaling measures had fair to excellent ranges except for the pelvis (height and depth, width), femur and tibia, which ranged from poor to excellent reliability (Table 2). Bland Altman plots of between session measures showed no systematic differences or proportional biases (Supplemental Figure 1).

For spine curvature between sessions, mean differences were not significantly different from zero, however the variability was larger for lordosis than kyphosis (Figure 4, Table 3). Both measures had excellent reliability with ICCs>0.75. Bland Altman plots of between session measures showed no systematic differences or proportional biases (Supplemental Figure 2).

The distribution of spine loading for neutral standing across T1 to L5 spine levels is shown in Figure 5. Subject-specific spine loading between sessions was not significantly different for all activities. Interquartile ranges and total range of mean difference were similar across all levels of the spine for most simulated activities (Figure 6, Supplemental Figure 3). The ICC values of spine loading from T1 to L5 were mostly excellent, with 91% of ICC point estimates being greater than 0.75 for all activities (Supplement Table 1). ICCs with point estimates ≤0.75 occurred in the upper thoracic spine, specifically T1 – T7 for extension and T1 – T3 for lateral bending (Supplemental Table 1).

Discussion

Models created from optoelectronic motion capture data showed excellent between-session reliability for thoracic and lumbar spine loading for the activities investigated in this study. Thoracic and lumbar spine curvature measures also had excellent reliability, and the scaled body segments showed fair to excellent reliability between sessions. This is the first study to determine the reliability of marker-derived spine loading from marker-based subject-specific whole-body musculoskeletal models.

We found a mean difference in pelvis width, measured as the distance between hip joint centers, ranging from −1.7cm and 1.3 cm. Another study in adolescents found that pelvis width mean difference ranged from −2.5cm to 1.7cm between sessions(Kainz et al., 2017). These differences are similar to the inter-examiner precision reported by Della Croce et al., where precision of pelvis marker placement was between 1.5–2.5cm, and precision of hip joint center (using Bell's method) was 1.8cm(Della Croce et al., 1999). In the femur and tibia, we found that mean differences ranged from −3.8 to 1.7cm and −3.2 to 3.2cm respectively. These ranges are slightly larger than those reported in adolescents by Kainz et al., where mean difference ranged from −2.3cm to 2.6cm for femur and −2.3 to 2.0cm in the tibia, however this may be partially explained by a larger amount of soft tissue over bony landmarks in adults, which would affect palpation reproducibility (Kainz et al., 2017). Our study's pelvis height and depth, scaled from the distance between mid-hip joint center and the L5/S1 joint, was one of the least reliable measurements, with a 95% confidence interval ranging from poor to excellent reliability. This reliability variable is difficult to compare with other studies, as it incorporates elements of both pelvis height and depth in one measure. However, it does enforce the notion that careful pelvis and lower limb marker placement is critical, as these errors may propagate to estimations of hip joint centers and the L5/S1 joint.

Skin-based marker data from the spine and torso can be used to estimate internal spine curvature, as would be measured from a sagittal radiographic image. We used previously published and validated methods to estimate thoracic kyphosis and lumbar lordosis from marker data and external spine curvature, and these methods reported larger errors in the lumbar spine than the thoracic spine between referenced and estimated joint centers(Nerot et al., 2018). This may provide rationale for the larger between-session variation in lumbar lordosis than thoracic kyphosis that was observed in this study. Other studies estimating spine curvature from marker data with different methods also found that lumbar lordosis reliability was equal or lower to that of thoracic kyphosis, and error (or coefficient of variation) was higher when comparing lordosis to kyphosis(Dunk et al., 2005; Mousavi et al., 2018; Muyor et al., 2017; Severijns et al., 2020). Prior studies comparing skin-based marker-derived spine curvature to radiographic curvature show moderate to good correlation (Grindle et al., 2020; Schmid et al., 2015; Zemp et al., 2014). In addition to reliability and accuracy of spine curvature, accuracy of marker placement on bony anatomical landmarks is important for assessment of spine curvature. Confirmation of marker placement with an objective imaging technique will help assess accuracy, and while our current study did not investigate accuracy of marker placement, prior studies in the lumbopelvic region have

shown that subject gender and BMI can affect placement accuracy, as well as experience level of the examiner (Cooper et al., 2013; Ferreira et al., 2017; Snider et al., 2011).

Our results suggest that compressive loading estimates have excellent between-session reliability across all levels of the spine and in different activities. The lowest ICCs were observed in the upper thoracic spine, perhaps because overall loading is lower in this region, making it relatively more sensitive to changes in the model that affect spinal loading outcomes. Mean differences between sessions show that 82% of our compressive spine loads had less than 50N of variation between sessions across all spine levels and most activities. The absolute minimum and maximum of mean differences in spine loading was −132N to 175N across all activities and levels. As we previously reported, spine curvature is an important determinant of spine loading(Bruno et al., 2017b). As such, across all activities except trunk extension, if spine loading between sessions changed by more than 15% at any level, this is largely explained by differences (>10%) in lordosis or kyphosis between sessions. This indicates the majority of our spine loading differences can be described, at least in part, by the differences in spine curvature, and that an accurate assessment and implementation of spine curvature is crucial for creating subject-specific musculoskeletal models of the spine.

This study has several limitations, including a limited sample size of 17 individuals. However, the sample includes men and women across an age range of 24–74 years, allowing the reliability results to be applicable across the majority of the adult population for both sexes. Markers were placed on subjects by multiple examiners, which may have introduced additional precision error into our study compared to if only one examiner placed markers on each subject for each session(Della Croce et al., 1999). Additionally, subject-specific spinal kinematics were not used for this study, as we sought to isolate the effects of marker placement on spine modeling. Moreover, dynamic activities were not examined and differences in subject spinal motions between sessions would also contribute to inter-session differences in spine loading. For instance, if different bending or lifting techniques were used, these motion differences will alter muscle activation and spine load(Bazrgari et al., 2007). Additionally, inherent trial-to-trial motion variability has been found to be responsible for 8–14% of the total variation in spine range of motion, and 14–33% of the total variation in spinal loads (Granata et al., 1999).

In conclusion, this is the first study to investigate how variation in the placement of anatomical markers affects the reliability of body segment scaling, estimated spine curvature, and resulting compressive spine loading outcomes when creating subject-specific musculoskeletal models. Importantly, the majority of between-session differences in spine loading in this study may be explained by differences in spine curvature applied to models, especially in lumbar lordosis. Thus accurate assessment of spine curvature is crucial for subject-specific modeling. Overall, this study supports the use of optoelectronic motion capture to create full-body musculoskeletal models that can estimate subject-specific spine loading. This information informs future studies on dynamic spine loading, which are important for gaining insight into mechanisms contributing to back pain, vertebral fractures and other musculoskeletal injuries.

Supplementary Material

Refer to Web version on PubMed Central for supplementary material.

Acknowledgements

The authors would like to acknowledge Rebecca Tromp and Javad Mousavi for their role in subject recruitment and data collection. This work was conducted with support from the National Institute on Aging (R00AG042458) and National Institute of Arthritis, Musculoskeletal and Skin Diseases (R01AR073019) of the National Institutes of Health, the Department of Orthopaedic Surgery at Beth Israel Deaconess Medical Center, and Harvard Catalyst | The Harvard Clinical and Translational Science Center (National Center for Advancing Translational Sciences, National Institutes of Health Award UL1 TR001102) and financial contributions from Harvard University and its affiliated academic healthcare centers. The content is solely the responsibility of the authors and does not necessarily represent the official views of Harvard Catalyst, Harvard University and its affiliated academic healthcare centers, or the National Institutes of Health. The study sponsors had no role in the study design, data collection, analysis, manuscript preparation, or the decision to submit the manuscript for publication.

References

Actis JA, Honegger JD, Gates DH, Petrella AJ, Nolasco LA, Silverman AK, 2018. Validation of lumbar spine loading from a musculoskeletal model including the lower limbs and lumbar spine. J. Biomech. 68, 107–114. 10.1016/j.jbiomech.2017.12.001 [PubMed: 29310946]

Anderson FC, Pandy MG, 2001. Dynamic optimization of human walking. J. Biomech. Eng. 123, 381–90. [PubMed: 11601721]

Anderson FC, Pandy MG, 1999. A dynamic optimization solution for vertical jumping in three dimensions. Comput. Methods Biomech. Biomed. Engin. 2, 201–231. 10.1080/10255849908907988 [PubMed: 11264828]

Bazrgari B, Shirazi-Adl A, Arjmand N, 2007. Analysis of squat and stoop dynamic liftings: Muscle forces and internal spinal loads. Eur. Spine J. 16, 687–699. 10.1007/s00586-006-0240-7 [PubMed: 17103232]

Beaucage-Gauvreau E, Robertson WSP, Brandon SCE, Fraser R, Freeman BJC, Graham RB, Thewlis D, Jones CF, 2019. Validation of an OpenSim full-body model with detailed lumbar spine for estimating lower lumbar spine loads during symmetric and asymmetric lifting tasks. Comput. Methods Biomech. Biomed. Engin. 22, 451–464. 10.1080/10255842.2018.1564819 [PubMed: 30714401]

Bruno AG, Bouxsein ML, Anderson DE, 2015. Development and Validation of a Musculoskeletal Model of the Fully Articulated Thoracolumbar Spine and Rib Cage. J. Biomech. Eng. 137, 1–10. 10.1115/1.4030408

Bruno AG, Burkhart K, Allaire B, Anderson DE, Bouxsein ML, 2017a. Spinal Loading Patterns from Biomechanical Modeling Explain the High Incidence of Vertebral Fractures in the Thoracolumbar Region. J. Bone Miner. Res. 32, 1282–1290. 10.1002/jbmr.3113 [PubMed: 28244135]

Bruno AG, Mokhtarzadeh H, Allaire BT, Velie KR, De Paolis Kaluza MC, Anderson DE, Bouxsein ML, 2017b. Incorporation of CT-based measurements of trunk anatomy into subject-specific musculoskeletal models of the spine influences vertebral loading predictions. J. Orthop. Res. 35, 2164–2173. 10.1002/jor.23524 [PubMed: 28092118]

Carhart MR, 2000. Biomechanical Analysis of Compensatory Stepping: Implications for Paraplegics Standing Via FNS. Arizona State University.

Cooper K, Alexander L, Hancock E, Smith FW, 2013. The use of pMRI to validate the identification of palpated bony landmarks. Man. Ther. 18, 289–293. 10.1016/j.math.2012.10.005 [PubMed: 23134685]

De Leva P, 1996. Adjustments to zatsiorsky-seluyanov's segment inertia parameters. J. Biomech. 29, 1223–1230. 10.1016/0021-9290(95)00178-6 [PubMed: 8872282]

Della Croce U, Cappozzo A, Kerrigan DC, 1999. Pelvis and lower limb anatomical landmark calibration precision and its propagation to bone geometry and joint angles. Med. Biol. Eng. Comput. 37, 155–161. 10.1007/BF02513282 [PubMed: 10396818]

Delp SL, Anderson FC, Arnold AS, Loan P, Habib A, John CT, Guendelman E, Thelen DG, 2007. OpenSim: Open-source software to create and analyze dynamic simulations of movement. IEEE Trans. Biomed. Eng. 54, 1940–1950. 10.1109/TBME.2007.901024 [PubMed: 18018689]

Delp SL, Loan JP, Hoy MG, Zajac FE, Topp EL, Rosen JM, 1990. An interactive graphics-based model of the lower extremity to study orthopaedic surgical procedures. IEEE Trans. Biomed. Eng. 37, 757–767. 10.1109/10.102791 [PubMed: 2210784]

Dunk NM, Lalonde J, Callaghan JP, 2005. Implications for the use of postural analysis as a clinical diagnostic tool: Reliability of quantifying upright standing spinal postures from photographic images. J. Manipulative Physiol. Ther. 28, 386–392. 10.1016/j.jmpt.2005.06.006 [PubMed: 16096037]

Ferreira APA, Póvoa LC, Zanier JFC, Machado DC, Ferreira AS, 2017. Sensitivity for palpating lumbopelvic soft- tissues and bony landmarks and its associated factors : A single-blinded diagnostic accuracy study. J. Back Musculoskelet. Rehabil. 30, 735–744. 10.3233/BMR-150356 [PubMed: 28453451]

Granata KP, Marras WS, Davis KG, 1999. Variation in spinal load and trunk dynamics during repeated lifting exertions. Clin. Biomech. 14, 367–375. 10.1016/S0268-0033(99)00004-2

Grindle D, Mousavi SJ, Allaire B, White A, Anderson DE, 2020. Validity of flexicurve and motion capture for measurements of thoracic kyphosis versus standing radiographic measurements. JOR Spine (Accepted).

Ignasiak D, Rüeger A, Sperr R, Ferguson SJ, 2018. Thoracolumbar spine loading associated with kinematics of the young and the elderly during activities of daily living. J. Biomech. 70, 175–184. 10.1016/j.jbiomech.2017.11.033 [PubMed: 29248192]

Kainz H, Hoang HX, Stockton C, Boyd RR, Lloyd DG, Carty CP, 2017. Accuracy and Reliability of Marker-Based Approaches to Scale the Pelvis, Thigh, and Shank Segments in Musculoskeletal Models. J. Appl. Biomech. 33, 354–360. 10.1123/jab.2016-0282 [PubMed: 28290736]

Krumm D, Cockcroft J, Zaumseil F, Odenwald S, Milani TL, Louw Q, 2016. Analytical evaluation of the effects of inconsistent anthropometric measurements on joint kinematics in motion capturing. Gait Posture46, 1–4. 10.1016/j.gaitpost.2016.01.024 [PubMed: 27131168]

Liu YK, Laborde JM, Van Buskirk WC, 1971. Inertial properties of a segmented cadaver trunk: their implications in acceleration injuries. Aerosp. Med. 42, 650–657. 10.1080/10643389.2012.728825 [PubMed: 5155151]

Mousavi SJ, Swann MC, White AP, Tromp R, Anderson DE, 2018. Between-session reliability of opto-electronic motion capture in measuring sagittal posture and 3-D ranges of motion of the thoracolumbar spine. J. Biomech. 79, 248–252. 10.1016/j.jbiomech.2018.08.033 [PubMed: 30213648]

Muyor JM, Arrabal-Campos FM, Martínez-Aparicio C, Sánchez-Crespo A, Villa-Pérez M, 2017. Test-retest reliability and validity of a motion capture (MOCAP) system for measuring thoracic and lumbar spinal curvatures and sacral inclination in the sagittal plane. J. Back Musculoskelet. Rehabil. 30, 1319–1325. 10.3233/BMR-169750 [PubMed: 29154267]

Nerot A, Skalli W, Wang X, 2018. Estimation of spinal joint centers from external back profile and anatomical landmarks. J. Biomech. 70, 96–101. 10.1016/j.jbiomech.2017.11.013 [PubMed: 29223495]

Pearsall DJ, Reid JG, Livingston L. a, 1996. Segmental inertial parameters of the human trunk as determined from computed tomography. Ann. Biomed. Eng. 24, 198–210. 10.1007/BF02667349 [PubMed: 8678352]

Peng J, Panda J, Van Sint Jan S, Wang X, 2015. Methods for determining hip and lumbosacral joint centers in a seated position from external anatomical landmarks. J. Biomech. 48, 396–400. 10.1016/j.jbiomech.2014.11.040 [PubMed: 25497377]

Raabe ME, Chaudhari AMW, 2016. An investigation of jogging biomechanics using the full-body lumbar spine model: Model development and validation. J. Biomech. 49, 1238–1243. 10.1016/j.jbiomech.2016.02.046 [PubMed: 26947033]

Rast FM, Graf ES, Meichtry A, Kool J, Bauer CM, 2016. Between-day reliability of three-dimensional motion analysis of the trunk: A comparison of marker based protocols. J. Biomech. 49, 807–811. 10.1016/j.jbiomech.2016.02.030 [PubMed: 26920506]

Richards JG, 1999. The measurement of human motion: A comparison of commercially available systems. Hum. Mov. Sci. 18, 589–602. 10.1016/S0167-9457(99)00023-8

Schmid S, Studer D, Hasler CC, Romkes J, Taylor WR, Brunner R, Lorenzetti S, 2015. Using skin markers for spinal curvature quantification in main thoracic adolescent idiopathic scoliosis: An explorative radiographic study. PLoS One10. 10.1371/journal.pone.0135689

Severijns P, Overbergh T, Thauvoye A, Baudewijns J, Monari D, Moke L, Desloovere K, Scheys L, 2020. A subject-specific method to measure dynamic spinal alignment in adult spinal deformity. Spine J. 20, 934–946. 10.1016/j.spinee.2020.02.004 [PubMed: 32058084]

Shrout PE, Fleiss JL, 1979. Intraclass correlations: Uses in assessing rater reliability. Psychol. Bull. 86, 420–428. 10.1037/0033-2909.86.2.420 [PubMed: 18839484]

Snider KT, Snider EJ, Degenhardt BF, Johnson JC, Kribs JW, 2011. Palpatory accuracy of lumbar spinous processes using multiple bony landmarks. J. Manipulative Physiol. Ther. 34, 306–313. 10.1016/j.jmpt.2011.04.006 [PubMed: 21640254]

Yamaguchi GT, Zajac FE, 1989. A planar model of the knee joint to characterize the knee extensor mechanism. J. Biomech. 22, 1–10. [PubMed: 2914967]

Zemp R, List R, Gul T, Elsig JP, Naxera J, Taylor WR, Lorenzetti S, 2014. Soft tissue artefacts of the human back: Comparison of the sagittal curvature of the spine measured using skin markers and an open upright MRI. PLoS One9, 1–8. 10.1371/journal.pone.0095426S

Figure 1:
Male (left) and female (right) full body thoracolumbar spine model created in OpenSim with 598 individual muscle fascicles. The male model is 175cm and 78kg. The female model is 163cm and 61 kg.

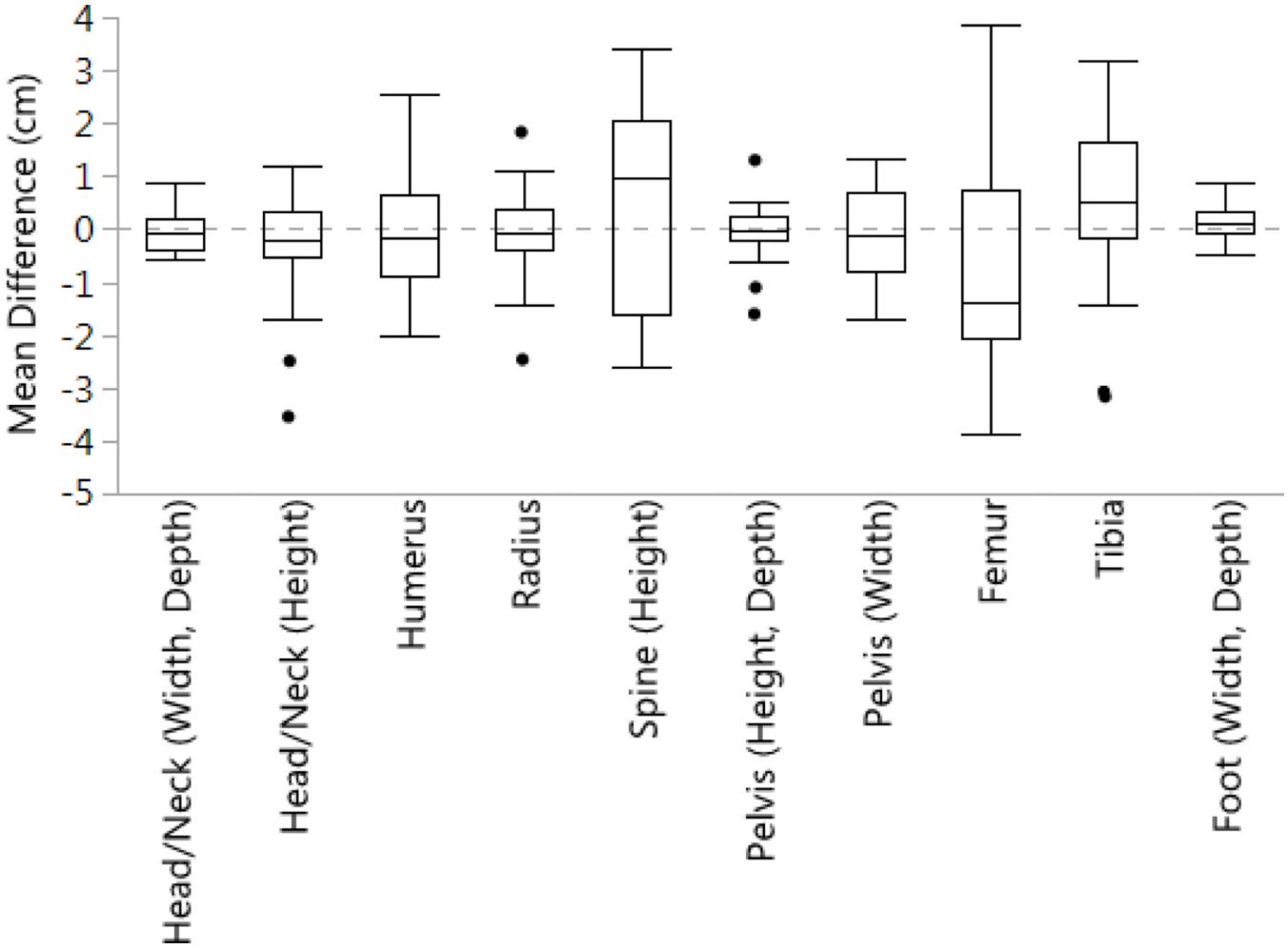

Figure 2:

Absolute difference (cm) in segment scaling of marker-estimated anthropometry between sessions. Box plots show median and inter-quartile range, with black dots representing outliers.

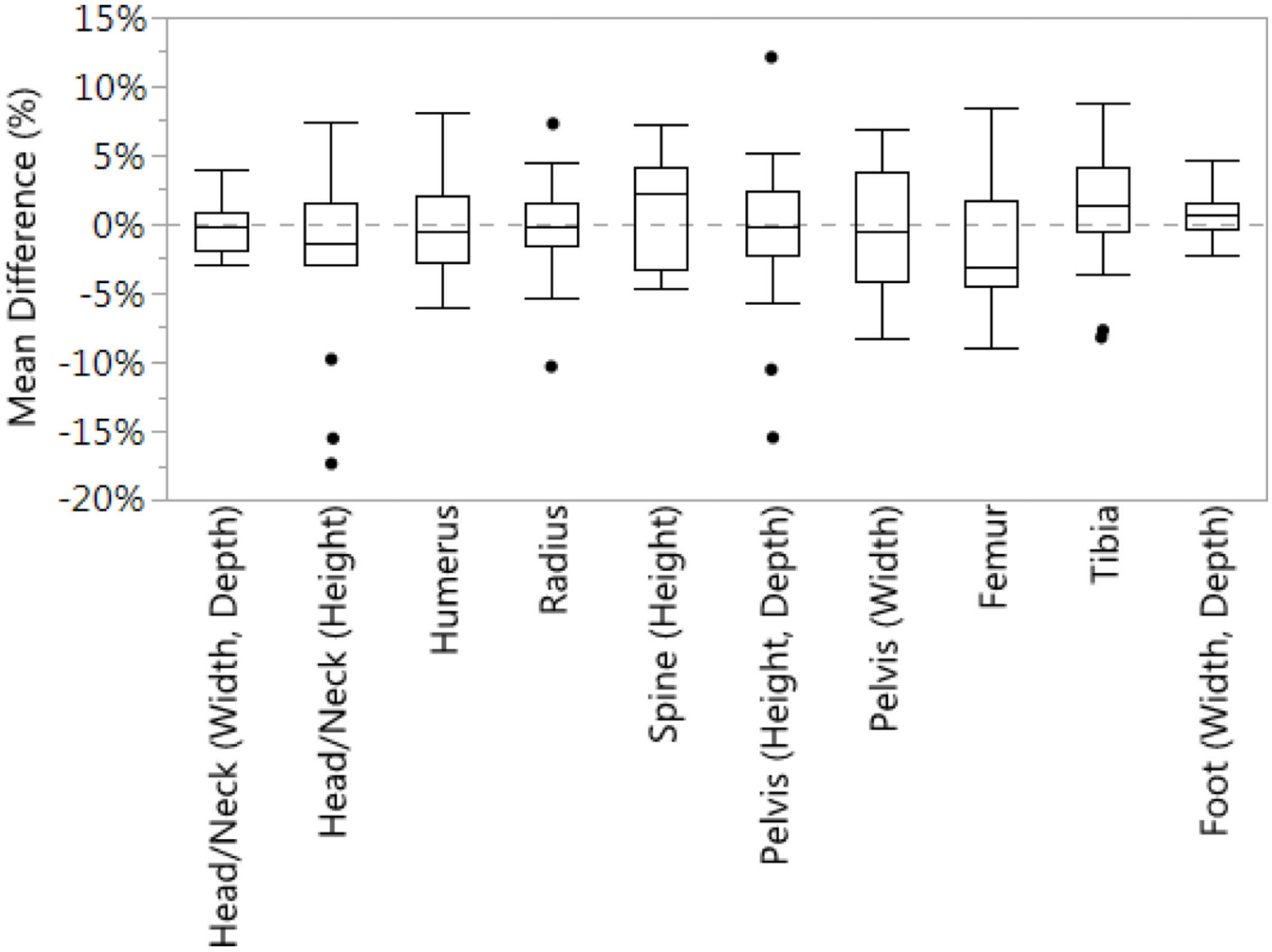

Figure 3:
Mean difference in percentage in segment scaling of marker-estimated anthropometry between sessions. Box plots show median and inter-quartile range, with black dots representing outliers.

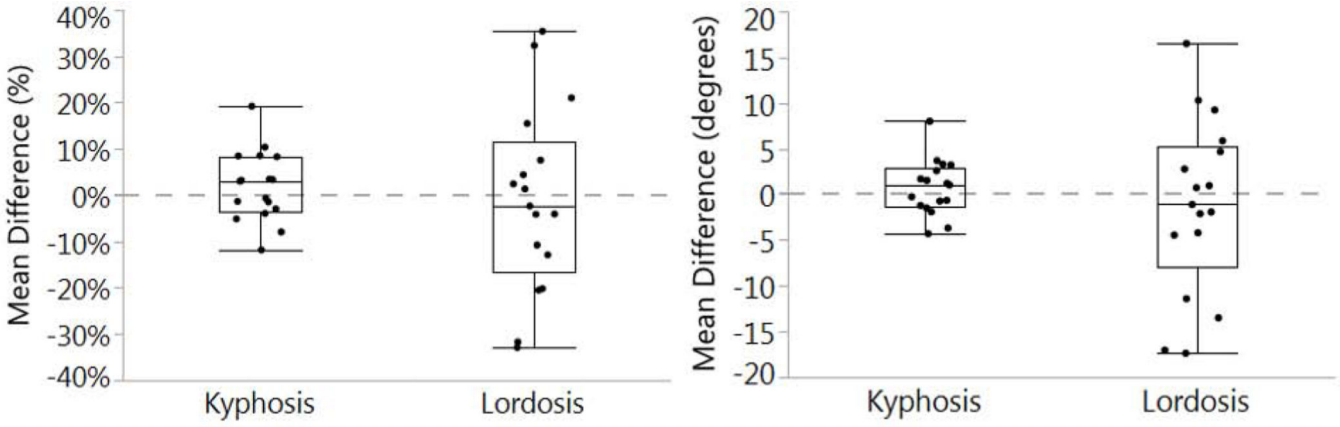

Figure 4:

Mean (%) (left) and absolute (degrees) (right) difference in marker-estimated spine curvature between sessions. Box plots show median and inter-quartile range, with black dots representing individual data points.

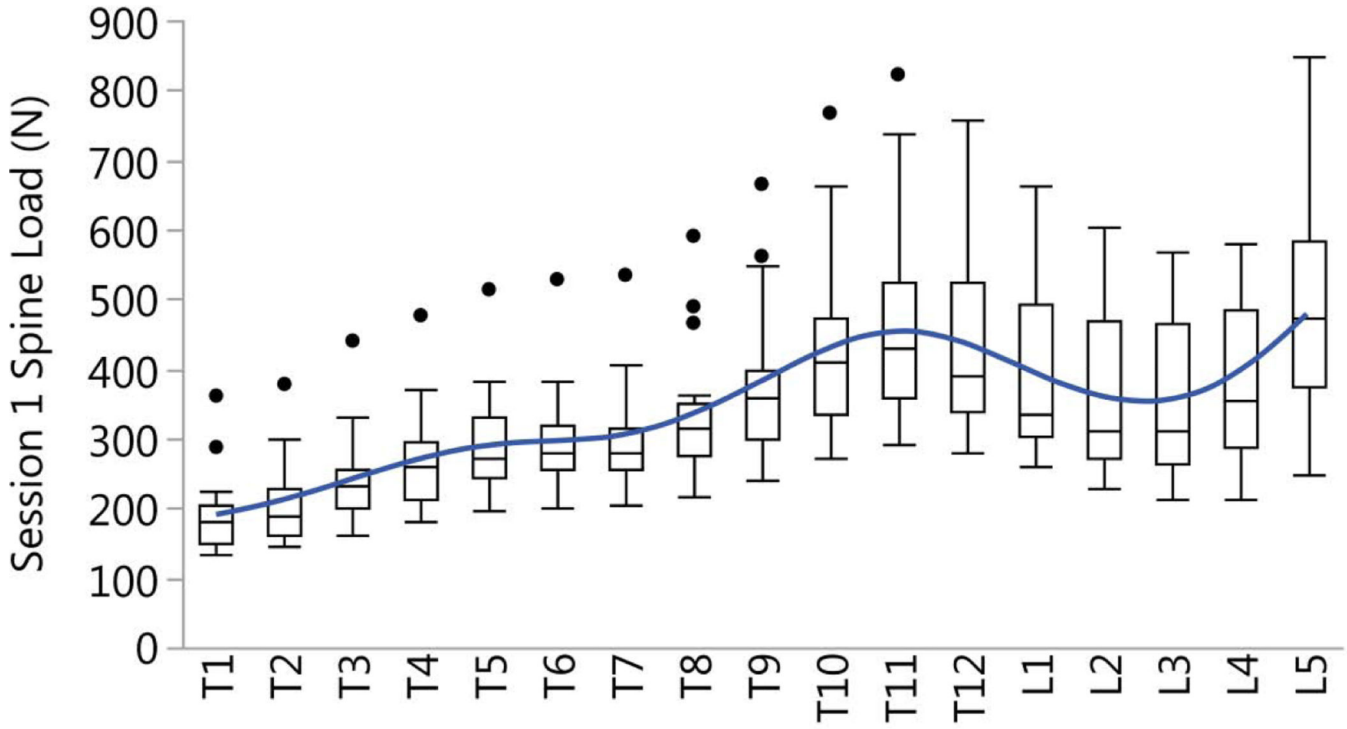

Figure 5:
Mean (blue line) of compressive spine load (N) during neutral standing in session 1, with box plots showing quartiles of data estimated at each spinal level (T1-L5). Black dots are representative of outliers.

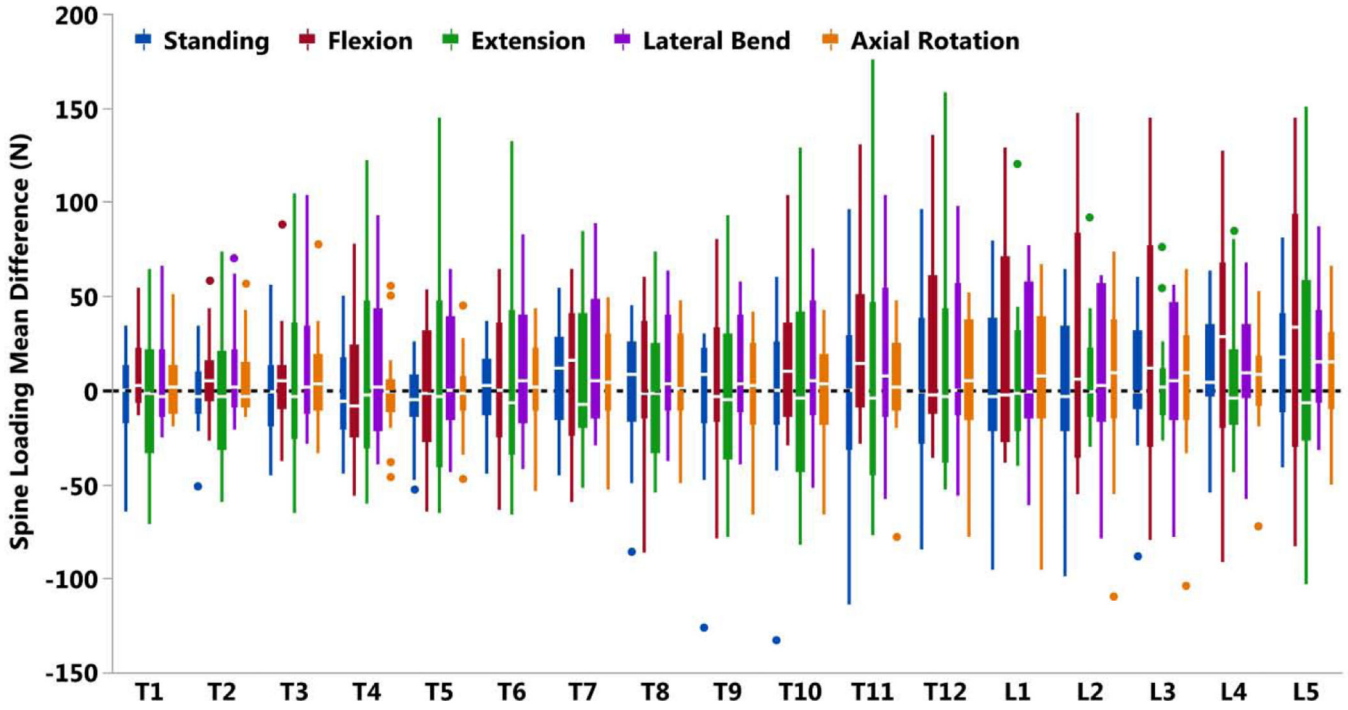

Figure 6:

Mean difference in compressive spine load across spinal levels during neutral standing, 45 degrees of trunk flexion, 15 degrees of trunk extension, 20 degrees of lateral bending and 45 degrees of axial rotation. Box plots show median, interquartile range and range. Outliers are represented by dots.

Table 1:

Segment scaling from marker data

Body Segment	Axis	Scaled to distance between:
Head/Neck	S-I	C7 marker to head center
	M-L, A-P	Diagonal distance between headband markers
Humerus	All	Acromion marker to lateral epicondyle of the humerus
Radius/Ulna	All	Lateral epicondyle of humerus to radial styloid process
Spine (T1-L5 vertebral bodies)	S-I	C7 marker to mid-PSIS
	M-L, A-P	Height scale factor
Pelvis/Sacrum	M-L	ASIS-ASIS and PSIS-PSIS
	S-I, A-P	Mid - hip joint center and L5/S1 joint
Femur	All	Hip joint center to knee joint center
Tibia/Fibula	All	Knee joint center to ankle joint center
Foot (Talus, Calcaneus, Toes)	M-L, A-P	Heel marker to 1st MTP joint (big toe)
	S-I	Height scale factor
All other bodies	All	Height scale factor

S-I: Superior-inferior (height), M-L: Medio-lateral (width), A-P: Anterior-posterior (depth)

Table 2:

Mean of Session 1 (SD), between-session ICCs (95% CI), and SEM of body segment scaling measures (in cm).

Measurement	Mean (SD)	ICC (95% CI)	SEM
Head/Neck (Width, Depth)	20.9 (0.9)	0.89 (0.71–0.96)	0.26
Head/Neck (Height)	18.2 (1.7)	0.75 (0.42–0.90)	0.90
Humerus	32.4 (1.8)	0.81 (0.55–0.92)	0.81
Radius	25.3 (1.8)	0.86 (0.66–0.95)	0.67
Spine (Height)	48.4 (3.7)	0.85 (0.63–0.94)	1.44
Pelvis (Height, Depth)	10.3 (0.6)	0.46 (−0.005–0.76)	0.43
Pelvis (Width)	19.2 (1.1)	0.65 (0.28–0.86)	0.63
Femur	43.8 (2.0)	0.56 (0.14–0.81)	1.30
Tibia	39.3 (2.3)	0.68 (0.33–0.87)	1.30
Foot (Width, Depth)	20.6 (1.2)	0.95 (0.87–0.98)	0.26

Table 3:

Mean of Session 1 (SD), between-session ICCs (95% CI), and SEM of marker-estimated spine curvature measures. Kyphosis is calculated as T4–T12 angle, and lordosis is calculated as L1–L5 angle. Units are in degrees.

Measurement	Mean (SD)	ICC (95% CI)	SEM (degrees)
Kyphosis	40.3 (7.1)	0.91 (0.77–0.96)	2.2
Lordosis	50.5 (15.2)	0.79 (0.52–0.92)	7.0